Electromagnetic spectral properties and Debye screening of a strongly magnetized hot medium

Aritra Bandyopadhyay,[*] Chowdhury Aminul Islam,[†] and Munshi G. Mustafa[‡]

Theory Division, Saha Institute of Nuclear Physics, HBNI, 1/AF Bidhan Nagar, Kolkata 700064, India

(Received 25 February 2016; revised manuscript received 1 August 2016; published 27 December 2016)

We evaluate the electromagnetic spectral function and its spectral properties by computing the one-loop photon polarization tensor involving quarks in the loop, particularly in a strong-field approximation compared to the thermal scale. When the magnetic scale is higher than the thermal scale the lowest Landau level (LLL) becomes an effectively $(1+1)$-dimensional strongly correlated system that provides a kinematical threshold based on the quark mass scale. Beyond this threshold the photon strikes the LLL and the spectral strength starts with a high value due to the dimensional reduction and then falls off with the increase of the photon energy due to LLL dynamics in a strong-field approximation. We obtain analytically the dilepton production rates from the LLL considering the lepton pair remains unaffected by the magnetic field when produced at the edge of a hot magnetized medium or it is affected by the magnetic field if produced inside a hot magnetized medium. For the latter case the production rate is of $\mathcal{O}[|eB|^2]$ along with an additional kinematical threshold due to the lepton mass. We also investigate the electromagnetic screening by computing the Debye screening mass and it depends distinctively on three different scales (mass of the quasiquark, temperature and the magnetic field strength) of a hot magnetized system. The mass dependence of the Debye screening supports the occurrence of a magnetic catalysis effect in the strong-field approximation.

DOI: 10.1103/PhysRevD.94.114034

I. INTRODUCTION

Ongoing relativistic heavy-ion collisions provide enough indications of the formation of the deconfined state of hadronic matter called quark-gluon plasma (QGP) and the nuclear matter under extreme conditions has been a subject of scrutiny. Recent studies [1–5] have revealed a captivating nature of noncentral heavy-ion collisions (HICs). They indicated that in such collisions, a very strong anisotropic magnetic field is generated in the direction perpendicular to the reaction plane, due to the relative motion of the ions themselves. The initial magnitude of this magnetic field can be very high ($eB \approx m_\pi^2$ at RHIC and $eB \approx 10m_\pi^2$ at LHC) at the time of the collision and then it decreases very fast, being inversely proportional to the square of time [6,7].[1]

The presence of an external anisotropic field in the medium subsequently requires a modification of the present theoretical tools that can be applied appropriately to investigate various properties of QGP. Intense research activity is underway to study the properties of strongly interacting matter in the presence of an external magnetic field, resulting in the emergence of several novel phenomena, e.g., the chiral magnetic effect [11–13], finite-temperature magnetic catalysis [14–16] and inverse magnetic catalysis [17–23], chiral- and color-symmetry broken/restoration phases [24–26], thermodynamic properties [27,28], refractive indices and decay constants [29,30] of mesons in a hot magnetized medium, soft photon production from the conformal anomaly [31,32] in HICs, the modification of dispersion properties in a magnetized hot QED medium [33], synchrotron radiation [8], and dilepton production from a hot magnetized QCD plasma [8–10,34] and also in a strongly coupled plasma in a strong magnetic field [35]. Also experimental evidence of photon anisotropy, provided by the PHENIX Collaboration [36], has posed a challenge for existing theoretical models. Subsequently some theoretical explanations are made by assuming the presence of a large anisotropic magnetic field in heavy-ion collisions [31]. This suggests that there is clearly an increasing demand to study the effects of intense background magnetic fields on various aspects and observables of noncentral heavy-ion collisions.

We know that the energy levels (orbitals) of a moving charged particle in the presence of a magnetic field get discretized, which are known as the Landau levels (LLs). One fascinating prospect of having a very strong background magnetic field is that only the lowest Landau level (LLL), whose energy is independent of the strength of the magnetic field, remains active in that situation. That is why, the LLL dynamics becomes solely important in the strong magnetic field approximation and the higher-order contributions, i.e., the radiative corrections play a significant role in this context, as it is the only way to get the B dependence in the LLL energy.

[*]aritra.bandyopadhyay@saha.ac.in
[†]chowdhury.aminulislam@saha.ac.in
[‡]munshigolam.mustafa@saha.ac.in

[1]However for a different point of view, see Refs. [8–10], where the time dependence of the magnetic field is shown to be adiabatic due to the high conductivity of the medium.

One of the primary ingredients of the theoretical tools for studying various properties of QGP is the n-point correlation function, which eventually determines the laws of propagation and the thermodynamic potential. Among them the electromagnetic correlation function is of particular interest because it is related to various physical quantities associated with the deconfined state of matter, such as the production rate of real and virtual photons (and dilepton pairs therefrom), which leave the fireball with minimum interaction. These electromagnetic probes are produced in every stage of the HICs. The dilepton spectra is a space-time integrated observable which has contributions coming from various stages of the collisions. Even though the dilepton may carry almost undistorted information about the stages in which they are produced, it would be very difficult to disentangle the contributions from different stages.

Processes like cyclotron emission which are usually abandoned in vacuum become active in the presence of an external magnetic field [37]. These processes affect the photon propagation and thus the spectral function. The spectral function or the spectral discontinuity of the electromagnetic correlator is directly related to the production rate of dileptons and photons. In vacuum, a full description of the polarization tensor in the presence of an external magnetic field has already been studied [38–41]. In this article we, first, would like to obtain the spectral representation of the electromagnetic correlation function in the presence of a strong background magnetic field at finite temperature. As a spectral property we then calculate the dilepton rate which is of immense importance especially in the scenario of noncentral heavy-ion collisions. At this point we note that the dilepton production rate under extreme magnetic fields has been addressed earlier by Tuchin [8–10] in a more phenomenological way. In order to estimate the dilepton production with logarithmic accuracy [9,10], a semiclassical Weiszäcker-Williams method [42] was employed to obtain the dilepton production rate by a hard quark as a convolution of the real photon decay rate with the flux of equivalent photons emitted by a fast quark. In this calculation it was approximated that the virtuality of photon has a negligible effect on photon emission and on dilepton production. Recently, Sadooghi and Taghinavaz [34] have analyzed in details the dilepton production rate for a magnetized hot and dense medium in a formal field-theoretic approach using the Ritus eigenfunction method [43]. In this article we use such a formal field-theoretic approach along with the Schwinger method [44] to obtain the electromagnetic spectral function and the dilepton rate in the strong-field approximation and compare our results with those of Ref. [34]. In addition we also discuss another interesting topic, namely the Debye screening, which could reveal some of the intriguing properties of the medium in the presence of a strong magnetic field.

The paper is organized as follows. In Sec. II we briefly review the setup, within the Schwinger formalism [44], required to compute the photon polarization tensor in the presence of a very strong background magnetic field along the z direction. In Sec. III we briefly discuss the vacuum spectral function and then obtain the in-medium photon polarization tensor and its spectral representation in the strong-field approximation. In Sec. IV we discuss how the dilepton rate for the LLL approximation would be modified and calculate the analytic expression for the dilepton production rate for various scenarios [9] in the strong magnetic field approximation. We take a closer look at the Debye screening in a strongly magnetized hot medium in Sec. V before concluding in Sec. VI.

II. SETUP

In the presence of a constant magnetic field pointing towards the z direction ($\vec{B} = B\hat{z}$), we first describe the charged fermion propagator. In coordinate space it can be expressed [44] as

$$S_m(x,x') = e^{\Phi(x,x')} \int \frac{d^4k}{(2\pi)^4} e^{-ik(x-x')} S_m(k), \qquad (1)$$

where $\Phi(x,x')$ is called the phase factor, which generally drops out in gauge-invariant correlation functions and the exact form of $\Phi(x,x')$ is not important in our problem. In momentum space the Schwinger propagator $S_m(k)$ can be written [44] as an integral over proper time s, i.e.,

$$\begin{aligned} iS_m(k) = \int_0^\infty ds \exp\left[is\left(k_\parallel^2 - m_f^2 - \frac{k_\perp^2}{q_f Bs}\tan(q_f Bs)\right)\right] \\ \times [(\not{k}_\parallel + m_f)(1 + \gamma_1\gamma_2 \tan(q_f Bs)) \\ - \not{k}_\perp (1 + \tan^2(q_f Bs))]. \end{aligned} \qquad (2)$$

Here, m_f and q_f are the mass[2] and *absolute charge* of the fermion of flavor f, respectively. The notation we have used in Eq. (2) and are going to follow throughout is

$$\begin{aligned} a^\mu &= a_\parallel^\mu + a_\perp^\mu; & a_\parallel^\mu &= (a^0, 0, 0, a^3); \\ a_\perp^\mu &= (0, a^1, a^2, 0), & & \\ g^{\mu\nu} &= g_\parallel^{\mu\nu} + g_\perp^{\mu\nu}; & g_\parallel^{\mu\nu} &= \mathrm{diag}(1,0,0,-1); \\ g_\perp^{\mu\nu} &= \mathrm{diag}(0,-1,-1,0), & & \\ (a\cdot b) &= (a\cdot b)_\parallel - (a\cdot b)_\perp; & (a\cdot b)_\parallel &= a^0b^0 - a^3b^3; \\ (a\cdot b)_\perp &= (a^1b^1 + a^2b^2), & & \end{aligned}$$

where $_\parallel$ and $\perp$ are, respectively, the parallel and perpendicular components, which are now separated out in the momentum-space propagator. After performing the

[2]Even if there is a dynamical mass generation in the system, one needs to make an appropriate modification. However, the fermion mass is generically represented by m_f in this calculation.

proper time integration [45], the fermion propagator in Eq. (2) can be represented as a sum over the discrete energy spectrum of the fermion

$$iS_m(k) = ie^{-\frac{k_\perp^2}{q_f B}} \sum_{n=0}^{\infty} \frac{(-1)^n D_n(q_f B, k)}{k_\parallel^2 - m_f^2 - 2nq_f B}, \tag{3}$$

with Landau levels $n = 0, 1, 2, \cdots$ and

$$D_n(q_f B, k) = (k_\parallel + m_f)\Bigg((1 - i\gamma^1\gamma^2)L_n\left(\frac{2k_\perp^2}{q_f B}\right) - (1 + i\gamma^1\gamma^2)L_{n-1}\left(\frac{2k_\perp^2}{q_f B}\right)\Bigg) - 4k_\perp L_{n-1}^1\left(\frac{2k_\perp^2}{q_f B}\right), \tag{4}$$

where $L_n^\alpha(x)$ is the generalized Laguerre polynomial written as

$$(1-z)^{-(\alpha+1)} \exp\left(\frac{xz}{z-1}\right) = \sum_{n=0}^{\infty} L_n^\alpha(x) z^n. \tag{5}$$

The energy level of charged fermions in the presence of a magnetic field follows from the pole of the propagator in Eq. (3) as

$$k_\parallel^2 - m_f^2 - 2nq_f B = k_0^2 - k_3^2 - m_f^2 - 2nq_f B = 0 \Rightarrow E_n = k_0 = \sqrt{k_3^2 + m_f^2 + 2nq_f B}. \tag{6}$$

It is seen that the energy along the direction of the magnetic field $(0, 0, B)$ is continuous but discretized along the transverse direction of the field. These discretized energy levels are so-called Landau levels, which are degenerate for each value of k_3. These Landau levels can affect the quantum fluctuations of the charged fermions in the Dirac sea at $T = 0$ and thermal fluctuations at $T \neq 0$, both of which arise as a response to the polarization of the electromagnetic field. These fluctuations are usually related to the electromagnetic polarization tensor or the self-energy of the photon, which at the one-loop level is expressed as

$$\Pi_{\mu\nu}(p) = -i\sum_f q_f^2 \int \frac{d^4k}{(2\pi)^4} \mathrm{Tr}_c[\gamma_\mu S_m(k)\gamma_\nu S_m(q)], \tag{7}$$

where p is the external momentum, and k and $q = k - p$ are the loop momenta. Tr_c represents both color and Dirac traces whereas the $\sum_f$ is over flavor because we have considered a two-flavor system ($N_f = 2$) of equal current quark mass ($m_f = m_u = m_d = 5$ MeV if not said otherwise).

The two point current-current correlator $C_{\mu\nu}(p)$ is related to the photon self-energy as

$$q_f^2 C_{\mu\nu}(p) = \Pi_{\mu\nu}(p), \tag{8}$$

with q_f is the electric charge of a given quark flavor f. The electromagnetic spectral representation is extracted from the imaginary part of the correlation function $C_\mu^\mu(p)$ as

$$\rho(p) = \frac{1}{\pi}\mathcal{I}mC_\mu^\mu(p) = \frac{1}{\pi}\mathcal{I}m\Pi_\mu^\mu(p)/q_f^2. \tag{9}$$

III. ELECTROMAGNETIC SPECTRAL FUNCTION AND ITS PROPERTIES IN THE PRESENCE OF A STRONG BACKGROUND MAGNETIC FIELD

In this section we will mainly investigate the nature of the in-medium electromagnetic spectral function in the presence of a very strong but constant magnetic field strength ($q_f B \gg T^2$), which could be relevant for initial stages of noncentral heavy-ion collisions, as a high-intensity magnetic field is believed to be produced there.

When the external magnetic field is very strong [46], $q_f B \to \infty$, it pushes all the Landau levels ($n \geq 1$) to infinity compared to the LLL with $n = 0$ (see Fig. 1). For the LLL approximation in the strong-field limit the fermion propagator in Eq. (3) reduces to a simplified form as

$$iS_{ms}(k) = ie^{-k_\perp^2/q_f B}\frac{k_\parallel + m_f}{k_\parallel^2 - m_f^2}(1 - i\gamma_1\gamma_2), \tag{10}$$

where k is the four-momentum and we have used the properties of the generalized Laguerre polynomial, $L_n \equiv L_n^0$ and $L_{-1}^\alpha = 0$. One could also get to Eq. (10) directly from Eq. (2) by putting $q_f B \to \infty$. The appearance of the projection operator $(1 - i\gamma_1\gamma_2)$ in Eq. (10) indicates that the spin of the fermions in the LLL are aligned along the field direction [1,45]. As $k_\perp^2 \ll q_f B$, one can see from Eq. (10) that an effective dimensional reduction from $(3 + 1)$ to $(1 + 1)$ takes place in the strong-field limit. As a

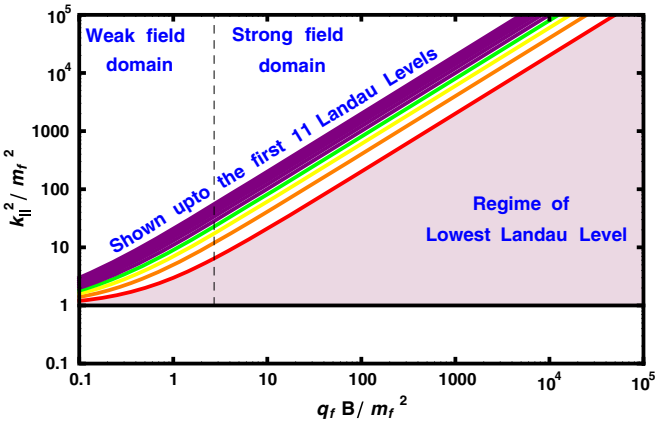

FIG. 1. Thresholds corresponding to a few Landau Levels are displayed as a function of $q_f B/m_f^2$. This threshold plot is obtained by solving $(\omega^2 - 4m_f^2 - 8nq_f B) = 0$ with zero photon momentum following energy conservation in a background magnetic field in general. Also the regime of the LLL in the strong magnetic field approximation is shown by the shaded area.

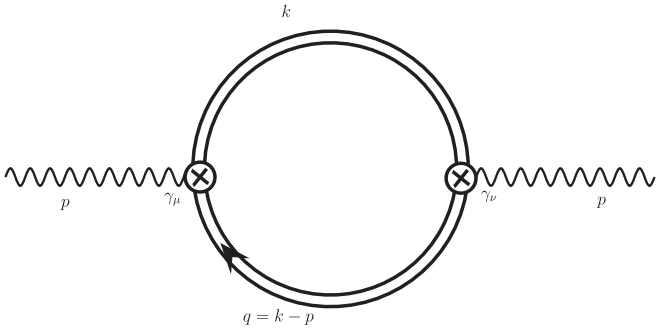

FIG. 2. Photon polarization tensor in the limit of the strong-field approximation.

consequence the motion of the charged particle is restricted in the direction perpendicular to the magnetic field but can move along the field direction in the LLL. This effective dimensional reduction also plays an important role in catalyzing the spontaneous chiral symmetry breaking [1,45] since the fermion pairing takes place in the LLL, which enhances the generation of fermionic mass through the chiral condensate in the strong-field limit at $T = 0$. The pairing dynamics is essentially $(1 + 1)$ dimensional where the fermion pairs fluctuate in the direction of the magnetic field. It is also interesting to see how these fermionic pairs respond to the electromagnetic fields. The fluctuation of fermion pairs in the LLL as shown in Fig. 2 is a response to the polarization of the electromagnetic field and would reveal various properties of the system in the presence of a magnetic field. Also the response to the electromagnetic field at $T \neq 0$ due to the thermal fluctuation of charged fermion pairs in the LLL would also be very relevant for the initial stages of noncentral heavy-ion collisions where the intensity of the generated magnetic field is very high.

Now in the one-loop photon polarization in Fig. 2 the effective fermionic propagator in the strong-field approximation is represented by a double line and the electromagnetic vertex remains unchanged[3] and is denoted by a crossed circle. As mentioned earlier the spin of the fermions in the LLL are aligned in the direction of the magnetic field because of the projection operator in Eq. (10). In a QED-like vertex with two fermions from the LLL the photon spin is equal to zero in the field direction [45] and there is no polarization in the transverse direction. Thus the longitudinal components [i.e., (0,3) components] of the QED vertex would only be relevant.

[3]This is not very apparent from the momentum-space effective propagator in Eq. (10) because of the presence of the projection operator. In Ref. [47] the Ward-Takahashi identity in the LLL for a fermion-antifermion-gauge boson in massless QED in the presence of a constant magnetic field was shown to be satisfied by considering the effective fermion propagator, the bare vertex and the free gauge boson propagator in the ladder approximation through the Dyson-Schwinger approach in a representation where the fermion mass operator is diagonal in momentum space.

Now in the strong-field limit the self-energy in Eq. (7) can be computed as

$$\begin{aligned}\Pi_{\mu\nu}(p)|_{sfa} &= -i\sum_f q_f^2 \int \frac{d^4k}{(2\pi)^4}\,\mathrm{Tr}_c[\gamma_\mu S_{ms}(k)\gamma_\nu S_{ms}(q)] \\ &= -iN_c\sum_f q_f^2 \int \frac{d^2k_\perp}{(2\pi)^2}\exp\left(\frac{-k_\perp^2 - q_\perp^2}{q_f B}\right) \\ &\quad\times \int \frac{d^2k_\parallel}{(2\pi)^2}\,\mathrm{Tr}\left[\gamma_\mu \frac{k\!\!\!/_\parallel + m_f}{k_\parallel^2 - m_f^2}(1 - i\gamma_1\gamma_2)\gamma_\nu \right. \\ &\quad\left.\times \frac{q\!\!\!/_\parallel + m_f}{q_\parallel^2 - m_f^2}(1 - i\gamma_1\gamma_2)\right], \end{aligned} \tag{11}$$

where "*sfa*" indicates the strong-field approximation and Tr represents only the Dirac trace. Now one can notice that the longitudinal and transverse parts are completely separated and the Gaussian integration over the transverse momenta can be done trivially, which leads to

$$\begin{aligned}\Pi_{\mu\nu}(p)|_{sfa} &= -iN_c\sum_f e^{-p_\perp^2/2q_fB}\frac{q_f^3 B}{\pi} \\ &\quad\times \int \frac{d^2k_\parallel}{(2\pi)^2}\frac{S_{\mu\nu}}{(k_\parallel^2 - m_f^2)(q_\parallel^2 - m_f^2)}, \end{aligned} \tag{12}$$

where the tensor structure $S_{\mu\nu}$ that originates from the Dirac trace is

$$S_{\mu\nu} = k_\mu^\parallel q_\nu^\parallel + q_\mu^\parallel k_\nu^\parallel - g_{\mu\nu}^\parallel((k\cdot q)_\parallel - m_f^2), \tag{13}$$

where the Lorentz indices μ and ν are restricted to longitudinal values and are forbidden to take any transverse values. In vacuum, Eq. (12) can be simplified using the Feynman parametrization technique [46], after which the structure of the photon polarization tensor can be written in compact form as

$$\Pi_{\mu\nu}(p) = \left(\frac{p_\mu^\parallel p_\nu^\parallel}{p_\parallel^2} - g_{\mu\nu}^\parallel\right)\Pi(p^2),$$

which directly implies that due to the current conservation, the two-point function is transverse. The scalar function $\Pi(p^2)$ is given by,

$$\begin{aligned}\Pi(p^2) &= N_c\sum_f \frac{q_f^3 B}{8\pi^2 m_f^2} e^{-p_\perp^2/2q_fB} \\ &\quad\times\left[4m_f^2 + \frac{8m_f^4}{p_\parallel^2}\left(1 - \frac{4m_f^2}{p_\parallel^2}\right)^{-1/2}\ln\frac{\left(1 - \frac{4m_f^2}{p_\parallel^2}\right)^{1/2} + 1}{\left(1 - \frac{4m_f^2}{p_\parallel^2}\right)^{1/2} - 1}\right]. \end{aligned} \tag{14}$$

We note that the lowest threshold (LT) for a photon to decay into a fermion and antifermion is provided by the energy

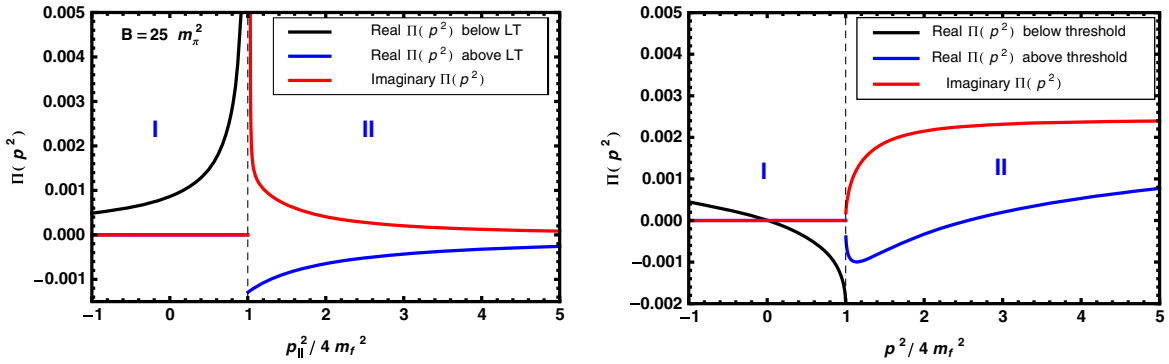

FIG. 3. Plot of the real and imaginary parts of $\Pi(p^2)$ as a function of the scaled photon momentum squared with respect to the LT in the kinematic regions I and II as discussed in the text in the presence of a strong magnetic field (left panel) and in the absence of a magnetic field (right panel).

conservation when the photon momenta $p_\parallel^2 (= \omega^2 - p_3^2) = (m_f + m_f)^2 = 4m_f^2$. Interestingly $\Pi(p^2)$ is singular in the presence of a magnetic field at this threshold. This is because of the appearance of the prefactor $\sqrt{1 - 4m_f^2/p_\parallel^2}$ in the denominator of the second term in Eq. (14) due to the dimensional reduction from $(3+1)$ to $(1+1)$ in the presence of the strong magnetic field. This behavior is in contrast to that in the absence of the magnetic field where a similar prefactor appears in the numerator [48]. Now, we explore $\Pi(p^2)$ physically in the following two domains around the LT, $p_\parallel^2 = 4m_f^2$:

(i) Region I, $p_\parallel^2 < 4m_f^2$: In this case with $a = \sqrt{4m_f^2/p_\parallel^2 - 1}$, let us write the logarithmic term in the second term of Eq. (14) as

$$\ln\left(\frac{ai+1}{ai-1}\right) = \ln\left(\frac{re^{i\theta_1}}{re^{i\theta_2}}\right) = i(\theta_1 - \theta_2), \qquad (15)$$

where $r = \sqrt{(1+a^2)}$, $\theta_1 = \arctan(a)$ and $\theta_2 = \arctan(-a)$. Thus in Eq. (14) the logarithmic term is purely imaginary but overall $\Pi(p^2)$ is real because of the prefactor $(1 - 4m_f^2/p_\parallel^2)^{-1/2}$ being imaginary. Even if we choose the limit $p_\parallel^2 < 0$, then also the whole term is real again, since the denominator of the logarithmic term, $\sqrt{1 - 4m_f^2/p_\parallel^2}$, is always greater than unity. So in the region $p_\parallel^2 < 4m_f^2$, $\Pi(p^2)$ is purely real.

(ii) Region II, $p_\parallel^2 > 4m_f^2$: Though in this limit the prefactor is real definite, but the denominator in the logarithmic term becomes negative and a complex number arises from it as $\ln(-x) = \ln|x| + i\pi$. Thus we get both real and imaginary contributions, i.e., $\mathcal{R}e\Pi(p^2)$ and $\mathcal{I}m\Pi(p^2)$, in this limit. The imaginary contribution is relevant for studying the spectral function and its spectral properties.

We now extract the vacuum spectral function in the presence of a strong magnetic field following Eq. (9) as

$$\rho\Big|_{sfa}^{\text{vacuum}} = \frac{1}{\pi}\mathcal{I}mC_\mu^\mu(p)\Big|_{sfa}^{\text{vacuum}} = N_c\sum_f \frac{q_f B m_f^2}{\pi^2 p_\parallel^2} e^{-p_\perp^2/2q_fB}\Theta(p_\parallel^2 - 4m_f^2) \times \left(1 - \frac{4m_f^2}{p_\parallel^2}\right)^{-1/2}. \qquad (16)$$

As can be seen the imaginary part is restricted by the LT, $p_\parallel^2 = 4m_f^2$. Below this threshold ($p_\parallel^2 < 4m_f^2$), $\Pi(p^2)$ is real and there is no electromagnetic spectral contribution in vacuum with a strong magnetic field as can be seen from region I in the left panel of Fig. 3. This implies that there is also no creation of a particle and antiparticle in vacuum below the LT because the width of the electromagnetic spectral function vanishes. Beyond the LT there is also a continuous contribution (blue solid line in region II) in the real part of $\Pi(p^2)$. As can be seen the real part of $\Pi(p^2)$ is continuous both below and above the LT but it has a discontinuity at the LT, $p_\parallel^2 = 4m_f^2$. Though we are interested in the imaginary part, we want to note that the real part can be associated with the dispersion property of a vector boson.[4] On the other hand the imaginary part of the electromagnetic polarization tensor is associated with interesting spectral properties of the system. So, beyond the LT ($p_\parallel^2 > 4m_f^2$) there is a nonzero continuous contribution to the electromagnetic spectral function as given by Eq. (16) and represented by a red solid line in region II in the left panel of Fig. 3. The right panel of Fig. 3 displays the analytic structure of the vacuum $\Pi(p^2)$ in the absence of a magnetic field [48]. In particular the comparison of the imaginary part of $\Pi(p^2)$ in the absence of the magnetic field with that in the

[4]This has been discussed in Refs. [49,50] without a magnetic field and in Ref. [45] with a magnetic field.

presence of the strong magnetic field reveals an opposite trend around the LT. This is due to the effect of dimensional reduction in the presence of the strong magnetic field. As a consequence the imaginary part of $\Pi(p^2)$ in the presence of a strong magnetic field would provide a very strong width to the photon that decays into a particle and antiparticle, *vis-à-vis* an enhancement of the dilepton production from the hot and dense medium produced in heavy-ion collisions. So far we have discussed some aspects of the electromagnetic polarization tensor with a strong background magnetic field in vacuum. Now we extend this to explore the spectral properties of a medium created in heavy-ion collisions with a strong background magnetic field.

In the present situation without any loss of information we can contract the indices μ and ν in Eq. (12), thus resulting in a further simplification as

$$\Pi^{\mu}_{\mu}(p)|_{sfa} = -iN_c\sum_f e^{-p_\perp^2/2q_fB}\frac{q_f^3B}{\pi} \times \int \frac{d^2k_\parallel}{(2\pi)^2}\frac{2m_f^2}{(k_\parallel^2-m_f^2)(q_\parallel^2-m_f^2)}. \quad (17)$$

At finite temperature this can be written by replacing the p_0 integral by a Matsubara sum as

$$\Pi^{\mu}_{\mu}(\omega,\mathbf{p})|_{sfa} = -iN_c\sum_f e^{-p_\perp^2/2q_fB}\frac{2q_f^3Bm_f^2}{\pi}\left(iT\sum_{k_0}\right) \times \int \frac{dk_3}{2\pi}\frac{1}{(k_\parallel^2-m_f^2)(q_\parallel^2-m_f^2)}. \quad (18)$$

We now perform the Matsubara sum using the mixed representation prescribed by Pisarski [51], where the trick is to dress the propagator in a way, such that it is spatial in the momentum representation, but temporal in the coordinate representation:

$$\frac{1}{k_\parallel^2-m_f^2} \equiv \frac{1}{k_0^2-E_k^2} = \int_0^\beta d\tau e^{k_0\tau}\Delta_M(\tau,k), \quad (19)$$

and

$$\Delta_M(\tau,k) = \frac{1}{2E_k}[(1-n_F(E_k))e^{-E_k\tau} - n_F(E_k)e^{E_k\tau}], \quad (20)$$

where $E_k = \sqrt{k_3^2+m_f^2}$ and $n_F(x) = (\exp(\beta x)+1)^{-1}$ is the Fermi-Dirac distribution function with $\beta = 1/T$. Using these, Eq. (18) can be simplified as

$$\begin{aligned}\Pi^{\mu}_{\mu}(\omega,\mathbf{p})|_{sfa} &= N_c\sum_f e^{\frac{-p_\perp^2}{2q_fB}}\frac{2q_f^3Bm_f^2}{\pi}T\sum_{k_0}\int\frac{dk_3}{2\pi}\int_0^\beta d\tau_1 \\ &\times\int_0^\beta d\tau_2 e^{k_0\tau_1}e^{(k_0-p_0)\tau_2}\Delta_M(\tau_1,k)\Delta_M(\tau_2,q) \\ &= N_c\sum_f e^{\frac{-p_\perp^2}{2q_fB}}\frac{2q_f^3Bm_f^2}{\pi}\int\frac{dk_3}{2\pi} \\ &\times\int_0^\beta d\tau e^{p_0\tau}\Delta_M(\tau,k)\Delta_M(\tau,q). \end{aligned} \quad (21)$$

Now the τ integral is trivially performed as

$$\begin{aligned}\Pi^{\mu}_{\mu}(\omega,\mathbf{p})|_{sfa} &= N_c\sum_f e^{\frac{-p_\perp^2}{2q_fB}}\frac{2q_f^3Bm_f^2}{\pi}\int\frac{dk_3}{2\pi} \\ &\times\sum_{l,r=\pm1}\frac{(1-n_F(rE_k))(1-n_F(lE_q))}{4(rl)E_kE_q(p_0-rE_k-lE_q)} \\ &\times[e^{-\beta(rE_k+lE_q)}-1]. \end{aligned} \quad (22)$$

One can now easily read off the discontinuity using

$$\mathtt{Disc}\left[\frac{1}{\omega+\sum_i E_i}\right]_\omega = -\pi\delta\left(\omega+\sum_i E_i\right), \quad (23)$$

which leads to

$$\begin{aligned}\mathcal{I}m\Pi^{\mu}_{\mu}(\omega,\mathbf{p})|_{sfa} &= -N_c\pi\sum_f e^{\frac{-p_\perp^2}{2q_fB}}\frac{2q_f^3Bm_f^2}{\pi}\int\frac{dk_3}{2\pi} \\ &\times\sum_{l,r=\pm1}\frac{(1-n_F(rE_k))(1-n_F(lE_q))}{4(rl)E_kE_q} \\ &\times[e^{-\beta(rE_k+lE_q)}-1]\delta(\omega-rE_k-lE_q). \end{aligned} \quad (24)$$

The general form of the delta function in Eq. (24) corresponds to four processes[5] for the choices of $r=\pm1$ and $l=\pm1$ as discussed below:

(1) $r=-1$ and $l=-1$ corresponds to a process with $\omega<0$, which violates energy conservation as all the quasiparticles have positive energies.

(2) (a) $r=+1$ and $l=-1$ corresponds to a process, $q\to q\gamma$, where a quark with energy E_k makes a transition to an energy E_q after emitting a timelike photon of energy ω. (b) $r=-1$ and $l=1$ corresponds to a case similar to (a). It is explicitly shown in the Appendix that both processes are not allowed by the phase space and the energy conservation. In other words, the production of a timelike photon from the one-loop photon polarization tensor is

[5]For the LLL we have explicitly checked that these four processes can also be seen from Eq. (4.19) in Ref. [34] where the Ritus method was used.

forbidden by the phase space and the energy conservation. However, we note here that these processes were somehow found to be nonzero for the LLL in Ref. [34].

(3) $r = 1$ and $s = 1$ corresponds to a process where a quark and an antiquark annihilate to a virtual photon, which is the only allowed process.

So, for the last case, one can write from Eq. (24)

$$\mathcal{I}m\Pi^{\mu}_{\mu}(\omega,\mathbf{p})|_{sfa} = N_c\pi\sum_f e^{\frac{-p_\perp^2}{2q_fB}}\frac{2q_f^3Bm_f^2}{\pi}\int\frac{dk_3}{2\pi}\delta(\omega-E_k-E_q)\frac{[1-n_F(E_k)-n_F(E_q)]}{4E_kE_q}. \tag{25}$$

After performing the k_3 integral using Eq. (A3) the spectral function in the strong-field approximation is finally obtained following Eq. (9) as

$$\rho\Big|_{sfa} = \frac{1}{\pi}\mathcal{I}mC^{\mu}_{\mu}(p)\Big|_{sfa} = N_c\sum_f\frac{q_fBm_f^2}{\pi^2p_\parallel^2}e^{-p_\perp^2/2q_fB}\Theta(p_\parallel^2-4m_f^2)\left(1-\frac{4m_f^2}{p_\parallel^2}\right)^{-1/2}[1-n_F(p_+^s)-n_F(p_-^s)], \tag{26}$$

where

$$p_\pm^s = \frac{\omega}{2}\pm\frac{p_3}{2}\sqrt{\left(1-\frac{4m_f^2}{p_\parallel^2}\right)}. \tag{27}$$

We note that the electromagnetic spectral function in the strong-field approximation obtained here in Eq. (26) using the Schwinger method has a factor $[1-n_F(p_+^s)-n_F(p_-^s)]$. This thermal factor appears when a quark and antiquark annihilate to a virtual photon in a thermal medium, which is the only process allowed by the phase space as shown in our calculation. In Ref. [34] besides this, there also appeared additional thermal factors due to the presence of the transition processes ($q\to q\gamma$) as discussed above in items 2(a) and 2(b) and in the Appendix.

The vacuum part in the presence of the strong magnetic field can be easily separated out from Eq. (26) as

$$\rho|^{\text{vacuum}}_{sfa} = N_c\sum_f\frac{q_fBm_f^2}{\pi^2p_\parallel^2}e^{-p_\perp^2/2q_fB}\Theta(p_\parallel^2-4m_f^2)\times\left(1-\frac{4m_f^2}{p_\parallel^2}\right)^{-1/2}, \tag{28}$$

which agrees with that obtained in Eq. (16).

We outline some of the important features of the spectral functions:

(i) In general the electromagnetic spectral function in Eq. (26) vanishes in the massless limit of quarks. This particular feature arises because of the presence of the magnetic field which reduces the system to $(1+1)$ dimensions. This can be further understood from the symmetry argument and is attributed to the CPT invariance of the theory [52]. Physically this observation further signifies that in $(1+1)$ dimensions an on-shell massless thermal fermion cannot scatter in the forward direction.

(ii) The threshold, $p_\parallel^2 = 4m_f^2$, for the LLL is independent of the magnetic field strength. It is also independent of T as $q_fB \gg T^2$ in the strong-field approximation. Like the vacuum case here also the spectral function vanishes below the threshold and there is no pair creation of a particle and antiparticle. This is because the polarization tensor is purely real below the threshold. This implies that the momentum of the external photon supplies energy and the virtual pair in the LLL becomes real via photon decay.

(iii) When the photon longitudinal momentum squared is equal to the LT, $p_\parallel^2 = 4m_f^2$, it strikes the LLL and the spectral strength diverges because of the factor $(1-4m_f^2/p_\parallel^2)^{-1/2}$ that appears due to the dimensional reduction. Since the LLL dynamics is $(1+1)$ dimensional, there is a dynamical mass generation [45,47] of the fermions through the mass operator (e.g. chiral condensate), which causes the magnetic-field-induced chiral symmetry breaking in the system. This suggests that the strong fermion pairing takes place in the LLL [45] even at the weakest attractive interaction between fermions in $(3+1)$ dimensions. A $(3+1)$-dimensional weakly interacting system in the presence of a strong magnetic field can be considered as a strongly correlated system in the LLL dynamics which is $(1+1)$ dimensional. In that case m_f should be related to the dynamical mass provided by the condensates [45,47]. One can incorporate it based on nonperturbative model calculations, and then LT will change accordingly.

(iv) The spectral strength starts with a high value for the photon longitudinal momentum $p_\parallel > 2m_f$ due to the dimensional reduction or LLL dynamics and then falls off with the increase of ω as there is nothing beyond the LLL in the strong-field approximation. To improve the high-energy behavior of the spectral function one requires the weak-field approximation ($T^2 \gg q_fB$).

In Fig. 4 the variation of the spectral function with photon energy ω is shown for different values of T in the left panel and for different values of magnetic field in the right panel. With the increase in T the spectral strength in the left panel gets depleted because of the presence of the

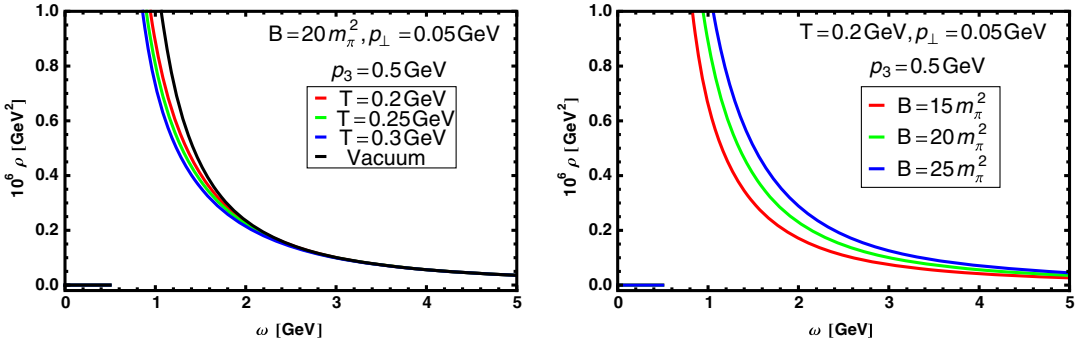

FIG. 4. Left panel: Variation of the spectral function with photon energy for different values of T at fixed B, $p_\perp$ and p_3. Right panel: Same as left panel but for different values of magnetic field at fixed T, $p_\perp$ and p_3. The value of the magnetic field is chosen in terms of the pion mass m_π.

thermal weight factor $[1 - n_F(p_+^s) - n_F(p_-^s)]$ as the distribution functions $n_F(p_\pm^s)$ increase with T which restricts the available phase space. Nevertheless the effect of temperature is small in the strong-field approximation as $q_f B \gg T^2$. On the other hand the spectral strength in the right panel increases with the increase of the magnetic field B as the spectral function is proportional to B.

In Fig. 5 the variation of the spectral function with photon energy ω is shown for three different values of the transverse momentum $p_\perp$. The spectral function is found to get exponentially suppressed with the gradually increasing value of $p_\perp$.

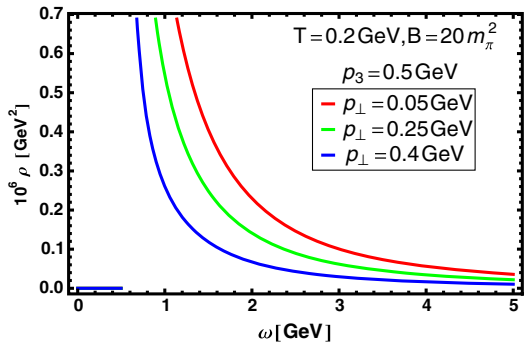

FIG. 5. Variation of the spectral function with photon energy ω for different values of transverse momentum at fixed B, T and p_3.

We also consider a special case where the external three-momentum (p) of the photon is taken to be zero and the simplified expression for the spectral function comes out to be,

$$\rho(\omega)\Big|_{sfa} = \frac{1}{\pi}\mathcal{I}mC_\mu^\mu(\omega, \mathbf{p}=0)\Big|_{sfa}$$
$$= N_c \sum_f \frac{q_f B m_f^2}{\pi^2\omega^2}\Theta(\omega^2 - 4m_f^2)\left(1 - \frac{4m_f^2}{\omega^2}\right)^{-1/2}$$
$$\times \left[1 - 2n_F\left(\frac{\omega}{2}\right)\right]. \quad (29)$$

In Fig. 6 the same things are plotted as in Fig. 4 but for a simplified case of zero external three-momentum of the photon. As can be seen from Eq. (29), here the value of the threshold is shifted to photon energy as $\omega = 2m_f$ and the shapes of the plots are slightly modified. In the following section as a spectral property we discuss the leading-order thermal dilepton rate for a magnetized medium.

IV. DILEPTON RATE

A. Dilepton rate in the absence of an external magnetic field

The dilepton multiplicity per unit space-time volume is given [53] as

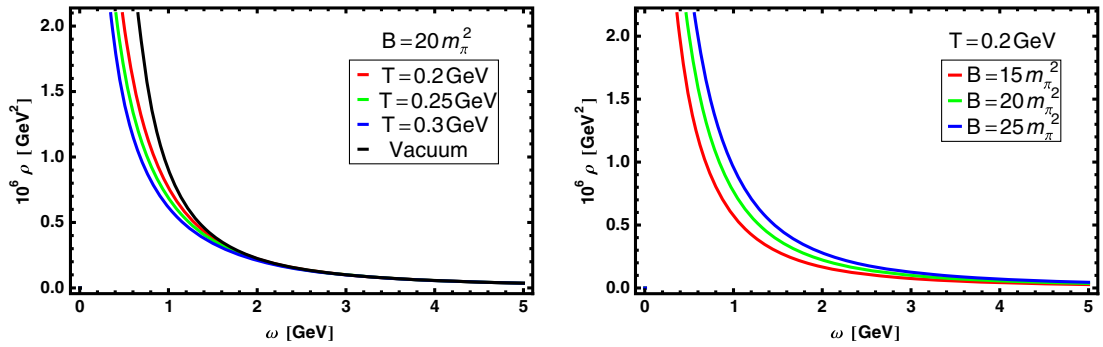

FIG. 6. Same as Fig. 4 but for zero external three-momentum (p) of the photon.

$$\frac{dN}{d^4x} = 2\pi e^2 e^{-\beta p_0} L_{\mu\nu}\rho^{\mu\nu}\frac{d^3\mathbf{q}_1}{(2\pi)^3 E_1}\frac{d^3\mathbf{q}_2}{(2\pi)^3 E_2}, \quad (30)$$

where $\mathbf{q}_i$ and E_i with $i = 1, 2$ are three-momentum and energy lepton pairs. The photonic tensor or the electromagnetic spectral function can be written as

$$\rho^{\mu\nu}(p_0,\mathbf{p}) = -\frac{1}{\pi}\frac{e^{\beta p_0}}{e^{\beta p_0}-1}\mathcal{I}m[D_R^{\mu\nu}(p_0,\mathbf{p})] \equiv -\frac{1}{\pi}\frac{e^{\beta p_0}}{e^{\beta p_0}-1}\frac{e_e^2}{p^4}\mathcal{I}m[C^{\mu\nu}(p_0,\mathbf{p})], \quad (31)$$

where e_e is the relevant electric charge, and $C^{\mu\nu}$ is the two-point current-current correlation function, whereas $D_R^{\mu\nu}$ represents the photon propagator. Here we used the relation [53]

$$e_e^2 C^{\mu\nu} = p^4 D_R^{\mu\nu}, \quad (32)$$

where e_e is the effective coupling.

Also the leptonic tensor in terms of Dirac spinors is given by

$$L_{\mu\nu} = \frac{1}{4}\sum_{\text{spins}}\text{tr}[\bar{u}(q_2)\gamma_\mu v(q_1)\bar{v}(q_1)\gamma_\nu u(q_2)] = q_{1\mu}q_{2\nu} + q_{1\nu}q_{2\mu} - (q_1\cdot q_2 + m_l^2)g_{\mu\nu}, \quad (33)$$

where $q_i \equiv (q_0, \mathbf{q}_i)$ is the four-momentum of the ith lepton. Now inserting $\int d^4p\delta^4(q_1+q_2-p) = 1$, one can write the dilepton multiplicity as

$$\frac{dN}{d^4x} = 2\pi e^2 e^{-\beta p_0}\int d^4p\delta^4(q_1+q_2-p)L_{\mu\nu}\rho^{\mu\nu} \times \frac{d^3q_1}{(2\pi)^3E_1}\frac{d^3q_2}{(2\pi)^3E_2}. \quad (34)$$

Using the identity

$$\int \frac{d^3q_1}{E_1}\frac{d^3q_2}{E_2}\delta^4(q_1+q_2-p)L_{\mu\nu} = \frac{2\pi}{3}\left(1+\frac{2m_l^2}{p^2}\right)\left(1-\frac{4m_l^2}{p^2}\right)^{1/2}(p_\mu p_\nu - p^2 g_{\mu\nu}) = \frac{2\pi}{3}F_1(m_l,p^2)(p_\mu p_\nu - p^2 g_{\mu\nu}), \quad (35)$$

the dilepton production rate comes out to be,

$$\frac{dN}{d^4x d^4p} = \frac{\alpha_{\text{em}}e_e^2}{12\pi^3}\frac{n_B(p_0)}{p^2}F_1(m_l,p^2)\left(\frac{1}{\pi}\mathcal{I}m[C_\mu^\mu(p_0,\mathbf{p})]\right), \quad (36)$$

where $n_B(p_0) = (e^{p_0/T}-1)^{-1}$. Now if we consider a two-flavor case, $N_f = 2$,

$$e_e^2 = \sum_f q_f^2 = \frac{5}{9}e^2 = \frac{5\times 4\pi\alpha_{\text{em}}}{9}, \quad (37)$$

and the dilepton rate can be written as

$$\frac{dN}{d^4x d^4p} = \frac{5\alpha_{\text{em}}^2}{27\pi^2}\frac{n_B(p_0)}{p^2}F_1(m_l,p^2)\left(\frac{1}{\pi}\text{Im}[C_\mu^\mu(p_0,\mathbf{p})]\right), \quad (38)$$

where the invariant mass of the lepton pair $M^2 \equiv p^2(= p_0^2 - |\mathbf{p}|^2 = \omega^2 - |\mathbf{p}|^2)$. We note that for a massless lepton ($m_l = 0$) $F_1(m_l, p^2) = 1$.

B. Dilepton rate in the presence of a strong external constant magnetic field

We first would like to note that the dileptons are produced in all stages of the hot and dense fireball created in heavy-ion collisions. They are produced at the leading order from the decay of a virtual photon through the annihilation of quark-antiquark pairs. In noncentral heavy-ion collisions an anisotropic magnetic field is expected to be generated in the direction perpendicular to the reaction plane, due to the relative motion of the heavy ions themselves (spectators). It is believed that the initial magnitude of this magnetic field can be very high at the time of the collision and then it decreases very fast [6,7]. The dilepton production from a magnetized hot and dense matter can generally be dealt with in three different scenarios [9,34]: 1) only the quarks move in a magnetized medium but not the final lepton pairs, 2) both quarks and leptons move in a magnetized medium and 3) only the final lepton pairs move in the magnetic field.

1. Quarks move in a strong magnetized medium but not the final lepton pairs

We emphasize that the case we consider here is interesting and very relevant to noncentral heavy-ion collisions, especially for the scenario of a fast decaying magnetic field [6,7] and also for lepton pairs produced late or at the edges of a hot and dense magnetized medium so that they are unaffected by the magnetic field. In this scenario only the electromagnetic spectral function $\rho^{\mu\nu}$ in Eq. (30) will be modified by the background constant magnetic field whereas the leptonic tensor $L_{\mu\nu}$ and the phase-space factors will remain unaffected. The dilepton rate for massless ($m_l = 0$) leptons can then be written from Eq. (38) as

$$\begin{aligned}\frac{dN}{d^4x d^4p} &= \frac{5\alpha_{\text{em}}^2}{27\pi^2}\frac{n_B(p_0)}{p^2}\left(\frac{1}{\pi}\mathcal{I}m[C_\mu^\mu(p_\parallel,p_\perp)]\right)_m \\ &= \frac{5\alpha_{\text{em}}^2}{27\pi^2}\frac{n_B(p_0)}{p^2}[\rho(p_\parallel,p_\perp)]_m \\ &= \frac{5N_c\alpha_{\text{em}}^2}{27\pi^4}n_B(\omega)\sum_f\frac{|q_fB|m_f^2}{p^2p_\parallel^2} \times e^{-p_\perp^2/2|q_fB|}\Theta(p_\parallel^2-4m_f^2)\left(1-\frac{4m_f^2}{p_\parallel^2}\right)^{-1/2} \times [1-n_F(p_+^s)-n_F(p_-^s)], \end{aligned} \quad (39)$$

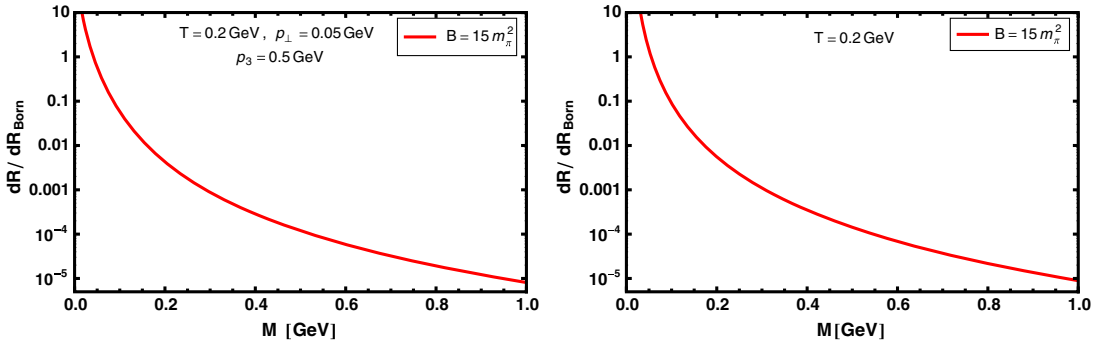

FIG. 7. Plot of the ratio of the dilepton rate in the strong magnetic field approximation to the Born rate (perturbative leading order) for both finite (left panel) and zero (right panel) external three-momentum of the photon.

where the electromagnetic spectral function $[\rho(p_\parallel, p_\perp)]_m$ in a hot magnetized medium comes from Eq. (26). The invariant mass of the lepton pair is $M^2 \equiv p^2(\omega^2 - |\mathbf{p}|^2) = \omega^2 - p_3^2 - p_\perp^2 = p_\parallel^2 - p_\perp^2$.

In Fig. 7 the ratio of the dilepton rate in the present scenario with the strong-field approximation to that of the perturbative leading-order (Born) dilepton rate is displayed as a function of the invariant mass. The left panel is for finite external photon momentum whereas the right panel is for zero external photon momentum. The features of the spectral function as discussed above are reflected in these dilepton rates. The LLL dynamics in the strong-field approximation enhances the dilepton rate as compared to the Born rate for a very low invariant mass ($\lesssim 100$ MeV), whereas at high mass it falls off very fast similar to that of the spectral function since there is no higher LL in the strong-field approximation as noted in point (iv). One requires the weak-field approximation ($q_f B \ll T^2$) to improve the high-mass behavior of the dilepton rate. We note that the enhancement found in the strong-field approximation in the rate will contribute to the dilepton spectra at low invariant mass, which is however beyond the scope of the present detectors involved in heavy-ion collisions experiments.

2. Both quark and lepton move in a magnetized medium in the strong-field approximation

This scenario is expected to be the most general one. To consider such a scenario the usual dilepton production rate given in Eq. (38) has to be supplemented with the appropriate modification of the electromagnetic and leptonic tensor along with the phase-space factors in a magnetized medium. Since we are interested in only the LLL, we briefly outline below the required modification[6] in the dilepton production rate only for the LLL:

(1) The phase-space factor in the presence of a magnetized medium gets modified [54] as

$$\frac{d^3\mathbf{q}}{(2\pi)^3 E} \to \frac{|eB|}{(2\pi)^2}\sum_{n=0}^{\infty}\frac{dq_z}{E} \tag{40}$$

where $d^2q_\perp = 2\pi|eB|$, e is the electric charge of the lepton and $\sum_{n=0}^{\infty}$ is over the LL. For a strong magnetic field one is confined in the LLL and $n=0$ only. The factor $|eB|/(2\pi)^2$ is the density of states in the transverse direction and is true for the LLL [45].

(2) The electromagnetic spectral function gets modified for the LLL as already discussed in Sec. III.

(3) In the presence of a constant magnetic field the spin of fermions is aligned along the field direction and the usual Dirac spinors $u(q)$ and $v(q)$ in Eq. (33) get modified [44,45] by $P_n u(\tilde{q})$ and $P_n v(\tilde{q})$ with $\tilde{q}^\mu = (q^0, 0, 0, q^3)$ and P_n is the projection operator at the nth LL. For the LLL it takes a simple form

$$P_0 = \frac{1 - i\gamma_1\gamma_2}{2}. \tag{41}$$

Now, the modification in the leptonic part in the presence of a strong magnetic field can be carried out as

$$\begin{aligned} L^m_{\mu\nu} &= \frac{1}{4}\sum_{\text{spins}}\text{tr}[\bar{u}(\tilde{q}_2)P_0\gamma_\mu P_0 v(\tilde{q}_1)\bar{v}(\tilde{q}_1)P_0\gamma_\nu P_0 u(\tilde{q}_2)] \\ &= \frac{1}{4}\text{tr}\left[(\tilde{q}_1 + m_l)\left(\frac{1-i\gamma_1\gamma_2}{2}\right)\gamma_\mu\left(\frac{1-i\gamma_1\gamma_2}{2}\right)\right. \\ &\quad \left.\times(\tilde{q}_2 - m_l)\left(\frac{1-i\gamma_1\gamma_2}{2}\right)\gamma_\nu\left(\frac{1-i\gamma_1\gamma_2}{2}\right)\right] \\ &= \frac{1}{2}[q^\parallel_{1\mu}q^\parallel_{2\nu} + q^\parallel_{1\nu}q^\parallel_{2\mu} \\ &\quad - ((q_1\cdot q_2)_\parallel + m_l^2)(g^\parallel_{\mu\nu} - g^\perp_{\mu\nu} - g_{1\mu}g_{1\nu} - g_{2\mu}g_{2\nu})]. \end{aligned} \tag{42}$$

(4) The insertion $\int d^2p^\parallel \delta^2(q_1^\parallel + q_2^\parallel - p^\parallel) = 1$ is required.

(5) The replacements[7] $d^2p^\perp = 2\pi|eB|$ and $d^4p = d^2p^\perp d^2p^\parallel$ are made.

[6] A detailed calculation for a more general case is in progress.

[7] The authors of Ref. [34] replaced $d^2p^\perp = V^{2/3}(\frac{eB}{2\pi})^2$, where V is the volume. This led to a different normalization factor in the dilepton rate in Ref. [34].

(6) The following identity is used:

$$2\pi|eB|\int\frac{dq_1^z}{E1}\int\frac{dq_2^z}{E2}\delta^2(q_1^\parallel+q_2^\parallel-p^\parallel)L^m_{\mu\nu}$$
$$=4\pi\frac{|eB|m_l^2}{(p_\parallel^2)^2}\left(1-\frac{4m_l^2}{p_\parallel^2}\right)^{-1/2}(p_\mu^\parallel p_\nu^\parallel-p_\parallel^2 g_{\mu\nu}^\parallel)$$
$$=\frac{4\pi}{(p_\parallel^2)^2}F_2(m_l,p_\parallel^2)(p_\mu^\parallel p_\nu^\parallel-p_\parallel^2 g_{\mu\nu}^\parallel). \quad (43)$$

Putting all these together, we finally obtain the dilepton production rate from Eq. (30) for the LLL as

$$\frac{dN^m}{d^4xd^4p}=\frac{\alpha_{em}e_e^2}{2\pi^3}\frac{n_B(p_0)}{p_\parallel^2p^4}F_2(m_l,p_\parallel^2)\left(\frac{1}{\pi}\mathcal{I}m[C_\mu^\mu(p_\parallel,p_\perp)]\right)_m, \quad (44)$$

and for two-flavor case ($N_f=2$) it becomes

$$\frac{dN^m}{d^4xd^4p}=\frac{10\alpha_{em}^2}{9\pi^2}\frac{n_B(p_0)}{p_\parallel^2p^4}|eB|m_l^2\left(1-\frac{4m_l^2}{p_\parallel^2}\right)^{-1/2}[\rho(p_\parallel,p_\perp)]_m$$
$$=\frac{10N_c\alpha_{em}^2}{9\pi^4}n_B(\omega)\sum_f\frac{|eB||q_fB|m_f^2m_l^2}{p_\parallel^4p^4}\Theta(p_\parallel^2-4m_l^2)$$
$$\times\left(1-\frac{4m_l^2}{p_\parallel^2}\right)^{-1/2}\Theta(p_\parallel^2-4m_f^2)\left(1-\frac{4m_f^2}{p_\parallel^2}\right)^{-1/2}$$
$$\times e^{-p_\perp^2/2|q_fB|}[1-n_F(p_+^s)-n_F(p_-^s)]. \quad (45)$$

We now note that the dilepton production rate in Eq. (45) is of $\mathcal{O}[|eB|^2]$ in the presence of a magnetic field B due to the effective dimensional reduction.[8] This dimensional reduction also renders a factor $1/\sqrt{1-4m_l^2/p_\parallel^2}$ in the leptonic part $L^m_{\mu\nu}$ that provides another threshold $p_\parallel^2\geq 4m_l^2$ in addition to that coming from the electromagnetic part $p_\parallel^2\geq 4m_f^2$. In general the mass of fermions in a magnetized hot medium will be affected by both temperature and magnetic field. The thermal effects [55,56] can be considered through thermal QCD and QED, respectively, for a quark ($\sim g^2T^2$; g is the QCD coupling) and lepton ($\sim e^2T^2$) whereas the magnetic effect comes through the quantized LL ($2n|q_fB|$). However, in the LLL ($n=0$), the magnetic effect on the mass correction vanishes in the strong-field approximation. Also in the strong-field approximation ($|q_fB|\gg T$), there could be dynamical mass generation through chiral condensates [45] of a quark and antiquark leading to magnetic-field-induced chiral symmetry breaking, which could play a dominant role. Nevertheless, the threshold will, finally, be determined by the effective mass $\tilde{m}=\max(m_l,m_f)$ as $\Theta(p_\parallel^2-4\tilde{m}^2)$ and the dilepton rate in the LLL reads as

$$\frac{dN^m}{d^4xd^4p}=\frac{10N_c\alpha_{em}^2}{9\pi^4}\sum_f\frac{|eB||q_fB|m_f^2m_l^2}{p_\parallel^4p^4}\Theta(p_\parallel^2-4\tilde{m}^2)$$
$$\times\left(1-\frac{4m_l^2}{p_\parallel^2}\right)^{-1/2}\left(1-\frac{4m_f^2}{p_\parallel^2}\right)^{-1/2}$$
$$\times e^{-p_\perp^2/2|q_fB|}n_B(\omega)[1-n_F(p_+^s)-n_F(p_-^s)], \quad (46)$$

where the kinematical factors agree but the prefactor $(10/\pi^4)$ and the thermal factor $n_B(\omega)[1-n_F(p_+^s)-n_F(p_-^s)]$ differ from those of Ref. [34] (the reasons for this were discussed in detail earlier). This restricts one to making a quantitative comparison of the dilepton rate with that obtained in Ref. [34]. We further note that a comparison with the experimental results or the results (dilepton spectra) obtained by Tuchin [9] needs a space-time evolution of the dilepton rate in a hot magnetized medium produced in heavy-ion collisions. A proper space-time evolution requires a hydrodynamic prescription in the presence of a magnetic field, which is indeed a difficult task and beyond the scope of this article.

We also note that the production rate for case 3) requires a modification of the leptonic tensor in a magnetized medium but the electromagnetic one remains unmagnetized. Since this is a rare possibility, we skip the discussion here but it can easily be obtained.

V. DEBYE SCREENING IN THE STRONG MAGNETIC FIELD APPROXIMATION

In this section we further explore the Debye screening mass in a strongly magnetized hot medium. In the static limit the Debye screening mass is obtained as

$$m_D^2=\Pi_{00}(\omega=0,|\vec{p}|\to 0). \quad (47)$$

Using Eq. (12) we get

$$\Pi_{00}|^{sfa}_{|\vec{p}|=0,\omega\to 0}$$
$$=N_c\sum_f\frac{q_f^3B}{\pi}\int_0^\infty\frac{dk_3}{2\pi}T\sum_{k_0}\frac{S_{00}}{(k_\parallel^2-m_f^2)^2}$$
$$=N_c\sum_f\frac{q_f^3B}{\pi}\int_0^\infty\frac{dk_3}{2\pi}\left[\frac{1}{4\pi i}\oint dk_0\frac{S_{00}[1-2n_F(k_0)]}{(k_0^2-E_k^2)^2}\right], \quad (48)$$

where, $E_k^2=k_3^2+m_f^2$ and at the limit of zero external three-momentum and vanishing external energy S_{00} comes out to be

[8] A factor $|eB|$ comes from the leptonic part whereas $\sum_f|q_fB|\propto|eB|$ from the electromagnetic spectral function involving quarks.

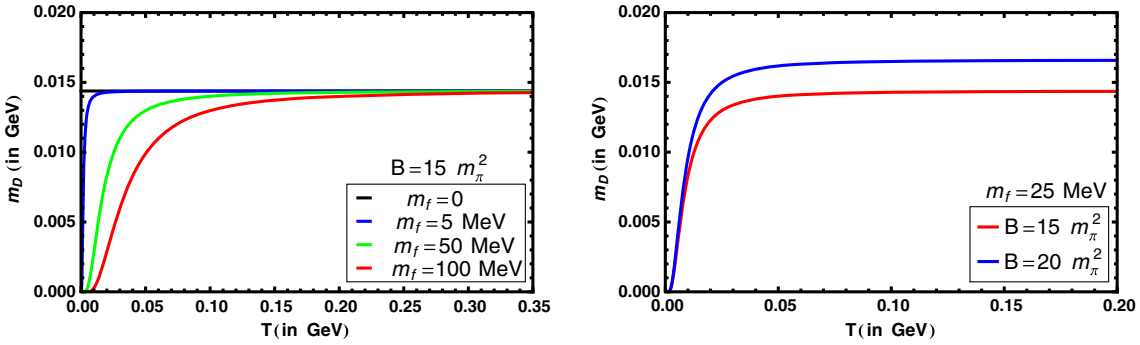

FIG. 8. Left panel: Variation of the Debye screening mass with temperature for different quark masses at a fixed value of B. Right panel: Comparison of the temperature variation of the Debye screening mass for two values of $B(=15m_\pi^2$ and $20m_\pi^2)$.

$$\begin{aligned} S_{00} &= k_0 q_0 + k_3 q_3 + m_f^2|_{|\vec{p}|=0,\omega\to 0} \\ &= k_0^2 + k_3^2 + m_f^2, \\ &= (k_0^2 - E_k^2) + 2E_k^2. \end{aligned} \tag{49}$$

Now, the k_0 integration can be divided into two parts as

$$I_1 = \frac{1}{4\pi i}\oint dk_0 \frac{[1-2n_F(k_0)]}{(k_0^2 - E_k^2)} = \frac{1-2n_F(E_k)}{2E_k}, \tag{50}$$

$$\begin{aligned} \text{and}\quad I_2 &= \frac{1}{4\pi i}\oint dk_0 \frac{2E_k^2[1-2n_F(k_0)]}{(k_0^2-E_k^2)^2} \\ &= 2E_k^2 \frac{d}{dk_0}\left(\frac{1-2n_F(k_0)}{(k_0+E_k)^2}\right)\Big|_{k_0=E_k} \\ &= -\frac{1-2n_F(E_k)}{2E_k} + \beta n_F(E_k)[1-n_F(E_k)], \end{aligned} \tag{51}$$

$$\therefore I_1 + I_2 = \beta n_F(E_k)[1-n_F(E_k)]. \tag{52}$$

From Eq. (48) the temporal part of the polarization tensor in the limit of zero external three-momentum (the long-wavelength limit) and vanishing external energy comes out to be

$$\Pi_{00}|^{sfa}_{|\vec{p}|=0,\omega\to 0} = N_c \sum_f \frac{q_f^3 B}{\pi T}\int_0^\infty \frac{dk_3}{2\pi} n_F(E_k)[1-n_F(E_k)]. \tag{53}$$

For the massive case ($m_f \neq 0$) this expression cannot be reduced further, analytically, by performing the k_3 integration. We evaluate it numerically to extract the essence of the Debye screening. On the other hand, for the massless case ($m_f = 0$) a simple analytical expression is obtained as

$$\begin{aligned} \Pi_{00}|^{sfa}_{|\vec{p}|,m_f=0,\omega\to 0} &= N_c \sum_f \frac{q_f^3 B}{\pi T}\int_0^\infty \frac{dk_3}{2\pi} n_F(k_3)[1-n_F(k_3)], \\ &= N_c \sum_f \frac{q_f^3 B}{\pi T}\frac{T}{4\pi} = N_c \sum_f \frac{q_f^3 B}{4\pi^2}. \end{aligned} \tag{54}$$

Before discussing the Debye screening we, first, note that the effective dimensional reduction in the presence of a strong magnetic field also plays an important role in catalyzing the spontaneous chiral symmetry breaking since the fermion pairing takes place in the LLL that strengthens the formation of spin-zero fermion-antifermion condensates. This enhances the generation of dynamical fermionic mass through the chiral condensate in the strong-field limit even at the weakest attractive interaction between fermions [1,45] at $T = 0$. The pairing dynamics is essentially $(1+1)$ dimensional where the fermion pairs fluctuate in the direction of the magnetic field. So, the zero-temperature magnetized medium is associated with two scales—the dynamical mass[9] m_f and the magnetic field B—whereas a hot magnetized medium is associated with three scales: the dynamical mass m_f, temperature T and the magnetic field B.

In the left panel of Fig. 8 the temperature variation of the Debye screening mass for quasiquarks in a strongly magnetized medium with $B = 15m_\pi^2$ and for different quark masses is shown. When the quark mass, $m_f = 0$, it is found to have a finite amount of Debye screening. This screening is independent of T because the only scale in the system is the magnetic field ($q_f B \gg T^2$), and the thermal scale gets canceled out exactly as found analytically in Eq. (54) in contrast to Ref. [57] where one needed to explicitly set the $T \to 0$ limit. We would like to note that when T drops below the phase transition temperature (T_c) the screening mass should, in principle, drop out. However, it is found to remain constant in the region $0 \le T \le T_c$, because of the absence of any mass scale in the system.

For massive quarks, the three scales became very distinct and an interesting behavior of the Debye screening mass is observed in the presence of a strong magnetic field. For a given m_f, as the temperature is gradually lowered below the value of the fermion mass ($T < m_f$), the quasiquark mass brings the Debye screening down as shown in the left panel

[9]As discussed before we still represent the dynamical mass scale by m_f.

of Fig. 8. Eventually the screening mass vanishes completely when $T = 0$. When $T \sim m_f$, there is a shoulder in the Debye screening and as soon as the temperature becomes higher than the value of m_f the screening becomes independent of other two scales ($m_f^2 \leq T^2 \leq q_f B$). So, in the presence of a strong magnetic field the Debye screening mass changes with temperature as long as $T < m_f$ and then saturates to a value determined by the strength of the magnetic field. Further as the quasiquark mass is increased the shoulder and the saturation point are pushed towards a higher T. The point at which the saturation takes place depends, particularly, on the strength of two scales, *viz.*, m_f and T associated with the hot magnetized system. In other words the dynamical mass generation catalyzes the spontaneous chiral symmetry breaking indicating magnetic catalysis [1,45,57] and in that case T_c will be enhanced as a reflection of the dimensionally reduced system in the presence of a strong magnetic field. Now we also note that if the thermal scale is higher than the magnetic scale ($T^2 \gg q_f B$), then the Debye screening will increase with T like the usual hot but unmagnetized medium. For this, however, one needs to employ a weak-field approximation where higher LL contributions will lead to an almost continuous system. This is because in a weak-field approximation ($q_f B \ll T^2$), the energy spacing between consecutive Landau levels, $[2(n+1)+1]q_f B - [2n+1]q_f B = 2q_f B$, gradually reduces with higher levels as shown in Fig. 1. In the right panel a comparison of the Debye screening mass is shown for massive quarks for two values of the magnetic field strength ($B = 15m_\pi^2$ and $20m_\pi^2$) and the screening is enhanced as it is proportional to B.

VI. CONCLUSION AND OUTLOOK

In this paper we have evaluated the in-medium electromagnetic spectral function by computing the imaginary part of the photon polarization tensor, in the presence of a magnetic field. We particularly dealt with the limiting case, where the magnetic field is very strong with respect to the thermal scale ($q_f B \gg T^2$) of the system. In this strong-field limit we have exploited the LLL dynamics that decouples the transverse and the longitudinal directions as a consequence of an effective dimensional reduction from $(3+1)$ dimensions to $(1+1)$ dimensions. The electromagnetic spectral function vanishes in the massless limit of quarks which implies that in $(1+1)$ dimensions an on-shell massless thermal fermion cannot scatter in the forward direction. Since the LLL dynamics is $(1+1)$ dimensional, the fermions are virtually paired up in the LLL providing a strongly correlated system, which could possibly enhance the generation of fermionic mass through the chiral condensate. So, these massive quarks could provide a kinematical threshold to the electromagnetic spectral function at longitudinal photon momentum, $p_\parallel^2 = 4m_f^2$. Below the threshold the photon polarization tensor is purely real and the electromagnetic spectral function does not exist resulting in no pair creation of a particle and antiparticle. This implies that the momentum of the external photon supplies energy to virtual fermionic pairs in the LLL, which become real via photon decay. At threshold the photon strikes the LLL and the spectral strength diverges due to the dimensional reduction, since a factor of $(1 - 4m_f^2/p_\parallel^2)^{-1/2}$ appears in the spectral function, in the strong-field approximation. The spectral strength starts with a high value for the photon longitudinal momentum $p_\parallel > 2m_f$ due to the dimensional reduction or LLL dynamics and then falls off with the increase of ω as there is nothing beyond the LLL in the strong-field approximation.

This strong-field approximation could possibly be very appropriate for the initial stages of the noncentral heavy-ion collisions where the intensity of the produced magnetic field is expected to be very high. As a spectral property we then obtained analytically the dilepton production rate for two scenarios: (i) when the quarks and antiquarks are affected by the hot magnetized medium but not the final lepton pairs and (ii) when both the quark and lepton are affected by the magnetized medium. In the former case the dilepton rate is $\mathcal{O}[|q_f B|]$ and follows the properties of the electromagnetic spectral function along with a kinematical threshold provided by the quark mass. For the latter case the rate was found to be $\mathcal{O}[|eB|^2$ with two kinematical thresholds provided by the quark (m_f) and lepton (m_l) masses. Since the dynamics in the LLL in the strong-field approximation is strongly correlated, the threshold will finally be determined by $\tilde{m} = \max(m_f, m_l)$.

We have also analyzed the electromagnetic screening effect through the Debye screening mass of the hot magnetized medium. This shows that there are three distinct scales in a hot magnetized medium, associated with the mass of the quasiquarks, the temperature of the medium and the background magnetic field strength. When the mass of the quasiquarks are much higher than the temperature, the Debye screening is negligible. As the temperature increases, the screening mass starts increasing, a shoulder-like structure appears when $T \sim m_f$, and then it saturates to a fixed value when $q_f B \gg T^2 \gg m_f^2$. In a strongly magnetized hot medium the Debye screening mass shows some interesting characteristics with temperature as long as $T \leq m_f$ and then saturates to a value determined by the strength of the magnetic field. The point at which the saturation takes place depends, especially, on the strength of the mass and temperature scales associated with a hot magnetized system. In the strong-field approximation the fermion pairing takes place in the LLL which could enhance the formation of quark-antiquark condensates, leading to a larger dynamical mass generation which catalyzes the spontaneous chiral symmetry breaking. This mass effect is reflected in the Debye screening as the shoulder and the saturation point are pushed towards a higher T when the quasiquark mass increases. The effective

dimensional reduction seems to plays an important role in catalyzing the spontaneous chiral symmetry breaking, which indicates an occurrence of the magnetic catalysis effect in the presence of a strong magnetic field.

ACKNOWLEDGMENTS

This work is supported by the Department of Atomic Energy (DAE), India through the project TPAES. The authors acknowledge fruitful discussion with A. Ayala and M. Strickland. A. B. gratefully acknowledges useful discussions with P. Chakraborty.

APPENDIX: PROCESSES WITH (A) $r=1, l=-1$ AND (B) $r=-1, l=1$

So, choosing first $r=1, l=-1$ we obtain from Eq. (24)

$$\mathcal{I}m\Pi^{\mu}_{\mu}(\omega,\mathbf{p})|_{\substack{r=1\\s=-1}} = N_c\pi\sum_f e^{\frac{-p_\perp^2}{2q_fB}}\frac{2q_f^3Bm_f^2}{\pi}\int\frac{dk_3}{2\pi}\frac{(1-n_F(E_k))(1-n_F(-E_q))}{4E_kE_q}\times[e^{-\beta(E_k-E_q)}-1]\delta(p_0-E_k+E_q). \tag{A1}$$

Now, using $1-n_F(-E_q)=n_F(E_q)$, one obtains

$$\mathcal{I}m\Pi^{\mu}_{\mu}(\omega,\mathbf{p})|_{\substack{r=1\\s=-1}} = N_c\sum_f e^{\frac{-p_\perp^2}{2q_fB}}\frac{2q_f^3Bm_f^2}{\pi}\int\frac{dk_3}{2}\delta(\omega-E_k+E_q)\frac{[n_F(E_k)-n_F(E_q)]}{4E_kE_q}. \tag{A2}$$

The k_3 integral can now be performed using the following property of the delta function:

$$\int_{-\infty}^{\infty}dp_3f(p_3)\delta[g(p_3)]=\sum_r\frac{f(p_{zr})}{|g'(p_{zr})|}, \tag{A3}$$

where the zeroes of the argument inside the delta function are called p_{zr}.

Now $\omega-E_k+E_q=0$ yields,

$$k_3^z=\frac{p_3}{2}\pm\frac{\omega}{2}\sqrt{1-\frac{4m_f^2}{(\omega^2-p_3^2)}},=\frac{p_3}{2}\pm\frac{\omega R}{2}, \tag{A4}$$

$$|g'(p_z)|=\left|\frac{E_k(k_3-p_3)-E_qk_3}{E_kE_q}\right|_{k_3=k_3^{z1},k_3^{z2}}, \tag{A5}$$

$$E_k|_{k_3=k_3^{z1}}=\frac{\omega}{2}+\frac{p_3R}{2},\qquad E_k|_{k_3=k_3^{z2}}=\frac{\omega}{2}-\frac{p_3R}{2}, \tag{A6}$$

$$E_q|_{k_3=k_3^{z1}}=\frac{\omega}{2}-\frac{p_3R}{2},\qquad E_q|_{k_3=k_3^{z2}}=\frac{\omega}{2}+\frac{p_3R}{2}, \tag{A7}$$

$$\text{and}\quad |E_k(k_3-p_3)-E_qk_3|_{k_3=k_3^{z1},k_3=k_3^{z2}}=\frac{\omega p_3}{2}(R^2-1), \tag{A8}$$

$$\begin{aligned}
\mathcal{I}m\Pi^{\mu}_{\mu}(\omega,\mathbf{p})|_{\substack{r=1\\s=-1}} &= N_c\sum_f e^{\frac{-p_\perp^2}{2q_fB}}\frac{2q_f^3Bm_f^2}{\pi}\sum_r\frac{[n_F(E_k)-n_F(E_q)]}{8E_kE_q}\times\left|\frac{E_kE_q}{E_k(k_3-p_3)-E_qk_3}\right|\Bigg|_{k_3=k_3^{zr}}\\
&= N_c\sum_f e^{\frac{-p_\perp^2}{2q_fB}}\frac{2q_f^3Bm_f^2}{\pi}\sum_r\frac{[n_F(E_k)-n_F(E_q)]}{8|E_k(k_3-p_3)-E_qk_3|}\Bigg|_{k_3=k_3^{zr}}\\
&= N_c\sum_f e^{\frac{-p_\perp^2}{2q_fB}}\frac{2q_f^3Bm_f^2}{4\pi\omega p_3(R^2-1)}\times[n_F(E_k|_{k_3=k_3^{z1}})-n_F(E_q|_{k_3=k_3^{z1}})+n_F(E_k|_{k_3=k_3^{z2}})-n_F(E_q|_{k_3=k_3^{z2}})]\\
&= N_c\sum_f e^{\frac{-p_\perp^2}{2q_fB}}\frac{2q_f^3Bm_f^2}{4\pi\omega p_3(R^2-1)}\times\left[n_F\left(\frac{\omega}{2}+\frac{p_3R}{2}\right)-n_F\left(\frac{\omega}{2}-\frac{p_3R}{2}\right)+n_F\left(\frac{\omega}{2}-\frac{p_3R}{2}\right)-n_F\left(\frac{\omega}{2}+\frac{p_3R}{2}\right)\right]\\
&= 0.
\end{aligned} \tag{A9}$$

Similarly, for the case (b) $r=-1$, $l=1$, the phase space also does not allow the corresponding process.

[1] I. A. Shovkovy, Lect. Notes Phys. **871**, 13 (2013).
[2] M. D'Elia, Lect. Notes Phys. **871**, 181 (2013).
[3] K. Fukushima, Lect. Notes Phys. **871**, 241 (2013).
[4] N. Mueller, J. A. Bonnet, and C. S. Fischer, Phys. Rev. D **89**, 094023 (2014).
[5] V. A. Miransky and I. A. Shovkovy, Phys. Rep. **576**, 1–209 (2015).
[6] A. Bzdak and V. Skokov, Phys. Rev. Lett. **110**, 192301 (2013).
[7] L. McLerran and V. Skokov, Nucl. Phys. **A929**, 184 (2014).
[8] K. Tuchin, Phys. Rev. C **87**, 024912 (2013).
[9] K. Tuchin, Phys. Rev. C **88**, 024910 (2013).
[10] K. Tuchin, Adv. High Energy Phys. **2013**, 490495 (2013).
[11] D. E. Kharzeev, L. D. McLerran, and H. J. Warringa, Nucl. Phys. **A803**, 227 (2008).
[12] K. Fukushima, D. E. Kharzeev, and H. J. Warringa, Phys. Rev. D **78**, 074033 (2008).
[13] D. E. Kharzeev, Ann. Phys. (Amsterdam) **325**, 205 (2010).
[14] J. Alexandre, K. Farakos, and G. Koutsoumbas, Phys. Rev. D **63**, 065015 (2001).
[15] V. P. Gusynin and I. A. Shovkovy, Phys. Rev. D **56**, 5251 (1997).
[16] D. S. Lee, C. N. Leung, and Y. J. Ng, Phys. Rev. D **55**, 6504 (1997).
[17] G. S. Bali, F. Bruckmann, G. Endrodi, Z. Fodor, S. D. Katz, S. Krieg, A. Schafer, and K. K. Szabo, J. High Energy Phys. 02 (2012) 044.
[18] V. G. Bornyakov, P. V. Buividovich, N. Cundy, O. A. Kochetkov, and A. Schafer, Phys. Rev. D **90**, 034501 (2014).
[19] N. Mueller and J. M. Pawlowski, Phys. Rev. D **91**, 116010 (2015).
[20] A. Ayala, M. Loewe, A. Z. Mizher, and R. Zamora, Phys. Rev. D **90**, 036001 (2014).
[21] A. Ayala, M. Loewe, and R. Zamora, Phys. Rev. D **91**, 016002 (2015).
[22] A. Ayala, M. Loewe, and R. Zamora, J. Phys. Conf. Ser. **720**, 012026 (2016).
[23] A. Ayala, C. A. Dominguez, L. A. Hernandez, M. Loewe, and R. Zamora, Phys. Lett. B **759**, 99 (2016).
[24] S. Fayazbakhsh and N. Sadooghi, Phys. Rev. D **83**, 025026 (2011).
[25] S. Fayazbakhsh and N. Sadooghi, Phys. Rev. D **82**, 045010 (2010).
[26] J. O. Andersen, W. R. Naylor, and A. Tranberg, arXiv:1411.1176.
[27] M. Strickland, V. Dexheimer, and D. P. Menezes, Phys. Rev. D **86**, 125032 (2012).
[28] J. O. Andersen, W. R. Naylor, and A. Tranberg, Rev. Mod. Phys. **88**, 025001 (2016).
[29] S. Fayazbakhsh, S. Sadeghian, and N. Sadooghi, Phys. Rev. D **86**, 085042 (2012).
[30] S. Fayazbakhsh and N. Sadooghi, Phys. Rev. D **88**, 065030 (2013).
[31] G. Basar, D. E. Kharzeev, and V. Skokov, Phys. Rev. Lett. **109**, 202303 (2012).
[32] A. Ayala, J. D. Castano-Yepes, C. A. Dominguez, and L. A. Hernandez, arXiv:1604.02713.
[33] N. Sadooghi and F. Taghinavaz, Phys. Rev. D **92**, 025006 (2015).
[34] N. Sadooghi and F. Taghinavaz, arXiv:1601.04887.
[35] K. A. Mamo, J. High Energy Phys. 08 (2013) 083.
[36] A. Adare *et al.* (PHENIX Collaboration), Phys. Rev. Lett. **109**, 122302 (2012).
[37] H. P. Rojas and A. E. Shabad, Ann. Phys. (N.Y.) **138**, 1 (1982).
[38] K. Hattori and K. Itakura, Ann. Phys. (Amsterdam) **330**, 23 (2013); **334**, 58 (2013).
[39] J. Chao, L. Yu, and M. Huang, Phys. Rev. D **90**, 045033 (2014).
[40] W.-y. Tsai, Phys. Rev. D **10**, 2699 (1974).
[41] W.-y. Tsai and T. Erber, Phys. Rev. D **10**, 492 (1974).
[42] J. Jackson, *Classical Electrodynamics*, 2nd ed. (Wiley, New York, 1975); R. Dalitz and D. Yennie, Phys. Rev. **105**, 1598 (1957).
[43] V. I. Ritus, Ann. Phys. (N.Y.) **69**, 555 (1972).
[44] J. Schwinger, Phys. Rev. **82**, 664 (1951).
[45] V. P. Gusynin, V. A. Miransky, and I. A. Shovkovy, Nucl. Phys. **B462**, 249 (1996).
[46] G. Calucci and R. Ragazzon, J. Phys. A **27**, 2161 (1994).
[47] E. J. Ferrer and V. de la Incera, Phys. Rev. D **58**, 065008 (1998).
[48] M. E. Peskin and D. V. Schroeder, *An Introduction to Quantum Field Theory* (Westview Press, Boulder, CO, 1995).
[49] Ch. A. Islam, S. Majumder, N. Haque, and M. G. Mustafa, J. High Energy Phys. 02 (2015) 011.
[50] C. Greiner, N. Haque, M. G. Mustafa, and M. H. Thoma, Phys. Rev. C **83**, 014908 (2011).
[51] R. D. Pisarski, Nucl. Phys. **B309**, 476 (1988).
[52] A. Das, R. R. Francisco, and J. Frenkel, Phys. Rev. D **86**, 047702 (2012).
[53] H. A. Weldon, Phys. Rev. D **42**, 2384 (1990).
[54] L. D. Landau and E. M. Lifshitz, *Quantum Mechanics: Non-relativistic Theory* (Pergamon Press, New York, 1977).
[55] J. I. Kapusta, *Finite-temperature Field Theory* (Cambridge University Press, Cambridge, England, 1989).
[56] M. Le Bellac, *Thermal Field Theory* (Cambridge University Press, Cambridge, England, 2000).
[57] J. Alexandre, Phys. Rev. D **63**, 073010 (2001).